Experimental investigation of a helical vortex pair

Dominic Schröder, Thomas Leweke, Ralf Hörnschemeyer, Eike Stumpf

EXPERIMENTAL INVESTIGATION OF A HELICAL VORTEX PAIR

D. Schröder*, T. Leweke†, R. Hörnschemeyer*, E. Stumpf*

* RWTH Aachen University, Institute of Aerospace Systems, 52062 Aachen, Germany

† CNRS, Aix-Marseille Université, Centrale Marseille, IRPHE, 13384 Marseille, France

Abstract

We present the results from an experimental study of helical vortex pairs. A one-bladed rotor in the hover regime is investigated in a recirculating water channel by means of dye visualizations and stereoscopic particle image velocimetry. In order to generate a system consisting of two concentrated, closely spaced, helical vortices, the rotor blade is modified with a parametric fin placed near its tip. An exchangeable blade tip geometry allows a fast variation of the fin parameters, such as its spanwise position, height and angle of attack, which influence the characteristics of the tip vortex pair. Through this parameter variation it was possible to obtain a configuration in which the two vortices have almost the same circulation. They are found to rapidly merge into a single helical wake vortex. A comparison of the cases without and with fin concerning wake evolution and vortex parameters reveals that, after one blade rotation, the merged vortex resulting from the initial vortex pair has a significantly larger core radius than the single tip vortex without fin. This finding may have relevance in the context of Blade-Vortex Interactions, where noise generation and fatigue from fluid-structure interactions depend strongly on the vortex core size.

Keywords

Rotor wake; Helical vortices; Merging; Dye visualization; Particle Image Velocimetry

NOMENCLATURE

Symbols

a	Vortex core radius	mm
b	Distance between vortex centres	mm
c	Chord length	cm
d	Distance to blade tip	mm
f	Rotor frequency	Hz
h	Height	mm
r	Rotor radius	cm
u_∞	Free-stream velocity	cm/s
v_t	Tangential velocity	cm/s
x, y, z	Cartesian coordinates	cm
Re	Reynolds number ($= 2\pi f r c_{\mathrm{tip}}/\nu$)	
α	Angle of attack	°
λ	Tip speed ratio ($= 2\pi f r/u_\infty$)	
ν	Kinematic viscosity	cm^2/s
ω	Vorticity	1/s
ϕ	Rotor phase	°
Γ	Circulation	cm^2/s

Subscripts

fin	Fin
m	Merged vortex
max	Maximum value
tip	Blade tip
tot	Total

Abbreviations

BVI	Blade-Vortex Interaction
PIV	Particle Image Velocimetry

1. INTRODUCTION

1.1. Background and Objective

Helical vortices occur in applications involving rotors. Rotating blades, like fixed wings, cause the formation of concentrated vortices at their tips, due to the pressure equalisation in the blade tip region. As a consequence of the combination of free-stream velocity and rotational movement, these vortices develop a characteristic helical geometry while propagating downstream. In current aerodynamic research, helical vortex wakes and their dynamics are of significant

importance for many practical issues. Regarding helicopters, the helical tip vortices and their interaction with a following blade (Blade-Vortex-Interaction, BVI) can generate unwelcome noise in certain flight regimes and cause unwanted vibrations of the structure [1]. The fatigue load incurred by a wind turbine, and its performance, can be affected adversely by the wake of another turbine placed upstream [2]. In both cases, the strength of the local velocity gradients, with the corresponding rapid change in local rotor blade airloads, is a crucial parameter. Consequently, the circulation and core radii of the tip vortices are vital elements affecting the strength of the interactions between these vortices and the following blades [3]. Minimizing the negative effects of BVI has been targeted in several studies over the past years, generating a variety of both active and passive applications. Various concepts involving active rotor control systems are presented in the review by Yung et al. [4]. The governing approach of passive systems is to influence the vortex parameters, in order to decrease the interaction with the following blade. The stability of both the entire rotor wake and a single helical vortex filament is of significant importance regarding possible BVI-reduction mechanisms. Various concepts for blade tip geometries and their influence on the vortices have been investigated, aiming at splitting or diffusing the tip vortex [5]. One operating principle of those tip shapes is to create multiple vortices that interact, resulting in a beneficial modification of the vortex parameters. The objective of the TWIN-HELIX project to gain a deeper physical understanding of the interaction phenomena occurring in such a closely spaced helical vortex system. In the present study, a special blade tip geometry is utilised to split up the single tip vortex in two separate vortices of almost equal circulation. The spatial and temporal evolution of both vortices is analysed in detail with experimental methods. Ultimately, the two separated vortices merge into a single final vortex. Mutual interactions in the vortex system influence this merging process. The goal here is the creation of a merged vortex with an increased core radius, combined with a reduced vorticity peak. An alteration of these vortex parameters in the described way holds a potential for reducing the negative effects associated with BVI.

1.2. Theoretical Aspects

1.2.1. Instabilities of Vortex Systems

The physics of vortex systems has been investigated in numerous studies. A review regarding the two-dimensional dynamics and the three-dimensional instabilities for co- and counter-rotating straight vortex pairs is presented in Ref. [6]. The instability mechanisms can be divided into two groups; despite the geometrical differences, this distinction can also be made for helical vortex systems [7]. The first mechanism causes a local perturbation of the whole vortex with minimal effects on the internal structure. Considering the associated wavelength of the perturbations in comparison to the vortex core diameter, the interactions are described as long-wavelength instabilities. Widnall [8] investigated the stability of a single helical vortex filament using self-induced velocities governed by the Biot-Savart law. An extension of this work to multiple interlaced helical vortices was made in the theoretical analysis by Gupta & Loewy [9]. The limitation of these studies is that the Biot-Savart integral for the flow induced by a helical filament does not have a closed form. An analytical solution for the velocity field induced by a helical filament was presented by Kawada [10] and Hardin [11]. Utilizing this result, Okulov [12], provided the analytical solution of the generalized stability problem for multiple helical vortices. An experimental study focussing on the long-wave instability of helical vortices was presented by Quaranta et al. [13, 14], involving the investigation of a single vortex and a configuration consisting of two interlaced helical vortices. The other group of instability mechanisms arises inside the vortex core, with perturbation wavelengths of the order of the core diameter. Moore & Saffman [15] deduced the resonance of Kelvin modes due to an imposed strain field as the reason for the instability. The present term used to describe this phenomenon, the elliptic instability, was introduced by Kerswell [16]. Leweke & Williamson [17] provided experimental evidence of the elliptic instability in straight vortex pairs without axial core flow. Meunier & Leweke [18] extended this work by studying the effect of three-dimensional instabilities on the vortex merging process. The effect of an axial core flow on the instability phenomena was investigated numerically by Roy et al. [19] for a co-rotating vortex pair. An experimental study of short-wave instabilities involving axial core flow was carried out by Roy et al. [20] for both counter- and co-rotating vortex pairs.

In helical vortex systems, Blanco-Rodríguez et al. [21] identified curvature and torsion as additional sources of short-wavelength instabilities responsible for internal core deformations. In a following study, Blanco-Rodríguez & Le Dizès [22] proved analytically that the curvature adds a contribution to the elliptic instability growth rate. Besides the elliptic instability, another short-wave phenomenon is found in vortices with a curved axis, the curvature instability. A comprehensive analysis of this instability phenomenon is presented by Fukumoto & Hattori [23] for a vortex ring. They extended their work to helical vortex systems including axial core flow [24, 25]. Blanco-Rodríguez & Le Dizès [26] presented an analytical investigation of the curvature instability in a helical vortex using the Batchelor model. A comparison between both short-wavelength instability mechanisms is provided by Hattori et al. [27], deducing that the vortex swirl has a crucial influence. Experimental work regarding short-wavelength instabilities in helical vortices can be found in the paper of Leweke et al. [7]. It is shown that the interaction between short-wave instabilities

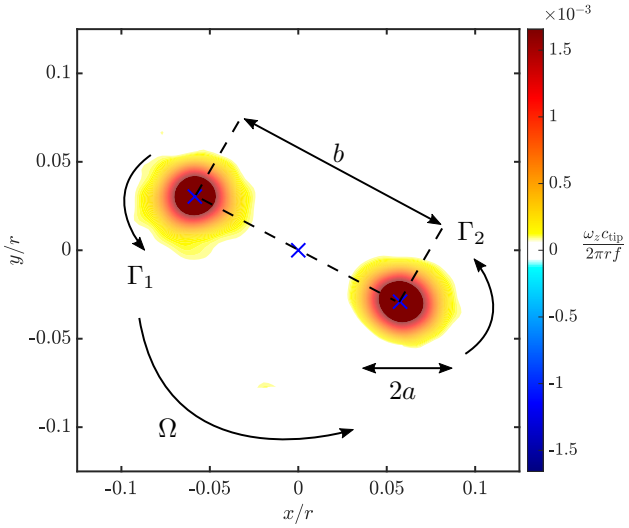

FIG 1. Vorticity field for two like-signed vortices of nearly equal strength (experimental data). Core radii a, separation distance b, circulations Γ_i and angular velocity Ω are marked, as in [29].

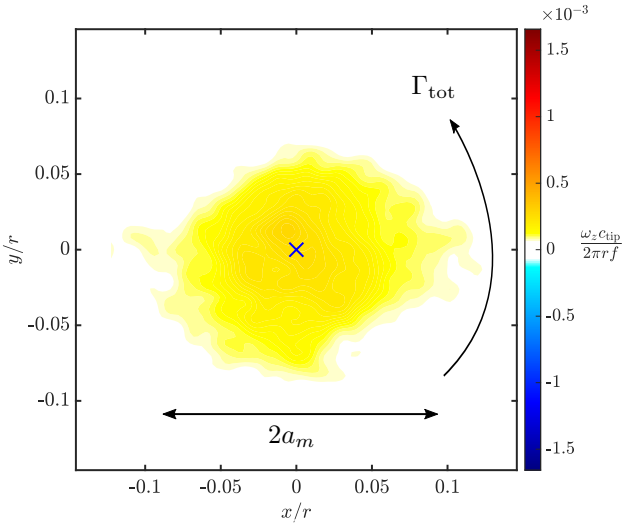

FIG 2. Vorticity distribution of the final vortex resulting from the merging of the vortices displayed in Fig. 1. The larger core radius and decreased vorticity peak are qualitatively visible.

and the long-wave deformation modes leads to a rapid disruption of the concentrated helical vortices, similar to the observations made for straight vortex pairs [17].

1.2.2. Vortex Merging

In addition to the mutual interactions, two like-signed vortices will ultimately merge to form a single vortex. The process of vortex merging and the underlying physics have been the topic of numerous studies over the past years, concerning the decay of turbulent coherent structures, possibly leading to the growth of larger structures. In their review paper, Hopfinger & van Heijst [28] refer to the merger process as the predominant mechanism of two-dimensional turbulence decay. Regarding the two-dimensional dynamics of merging, Leweke et al. [6] give a detailed description of possible configurations. Interpreting the vortices as point vortices with the circulation bound in the centres, two separated like-sign vortices of equal strength rotate around each other at an angular velocity $\Omega = (\Gamma_1 + \Gamma_2)/(2\pi b^2)$, which depends on the circulations Γ_i and the separation distance b. An example of a co-rotating vortex pair is shown in Fig. 1. In each vortex core, the presence of the respective other vortex induces a deformation of the streamlines into ellipses during the merging process. Due to the viscous diffusion of vorticity, the radii a of the vortices grow slowly, inducing an increase of the ratio a/b. After reaching a critical value, the two vortex cores move swiftly towards each other, deform rapidly and ultimately merge into one vortex. The critical value for the beginning of merging is typically $a/b \approx 0.24$ [6]. Experimental dye visualizations and numerical results for the two-dimensional evolution are provided in [30]. Melander et al. [31], Meunier & Leweke [32,33] and Cerretelli & Williamson [29] divided the complete merging process into four different stages, according to the temporal evolution of the vortex separation distance b. During the 'first diffusive stage', the separation distance remains essentially constant. It is followed by the 'convective stage', which is characterised by a rapid decrease of this distance. In the next phase, the 'second diffusive stage', the separation decreases more slowly. The merging process is completed in the 'merged diffusive stage', where only a single vorticity peak can be detected and a relaxation towards an axisymmetric shape takes place. Considering the characteristic vortex parameters of the merged vortex, the final core radius is widened and a decrease of both the maximum tangential velocity and the vorticity peak is observed [30]. Fig. 2 shows the merged vortex resulting from the two distinct vortices displayed in Fig. 1.

The physical explanation for the movement of the vortices towards each other is found by decomposing the total vorticity field into symmetric and antisymmetric components. The velocity pushing the vortex cores together is associated with the antisymmetric vorticity field, as shown by Cerretelli & Williamson [29]. Detailed studies governing the physics of vortex merging involving experimental, numerical and theoretical methods are presented in [29] and [30]. Merging is strongly affected by the presence of short-wavelength instabilities. Compared to merging without any internal instabilities, it is a more complex three-dimensional process. Meunier et al. [18, 32] pointed out that the criterion for onset and the characteristic parameters of the final merged vortex are strongly affected by the instabilities. The critical ratio a/b initialising the merging process for three-dimensional merging was found to be smaller than the corresponding value for the two-dimensional case. In addition, instability influence leads to a larger core size than in the absence of an instability, and to a greater decrease of the maximum tangential

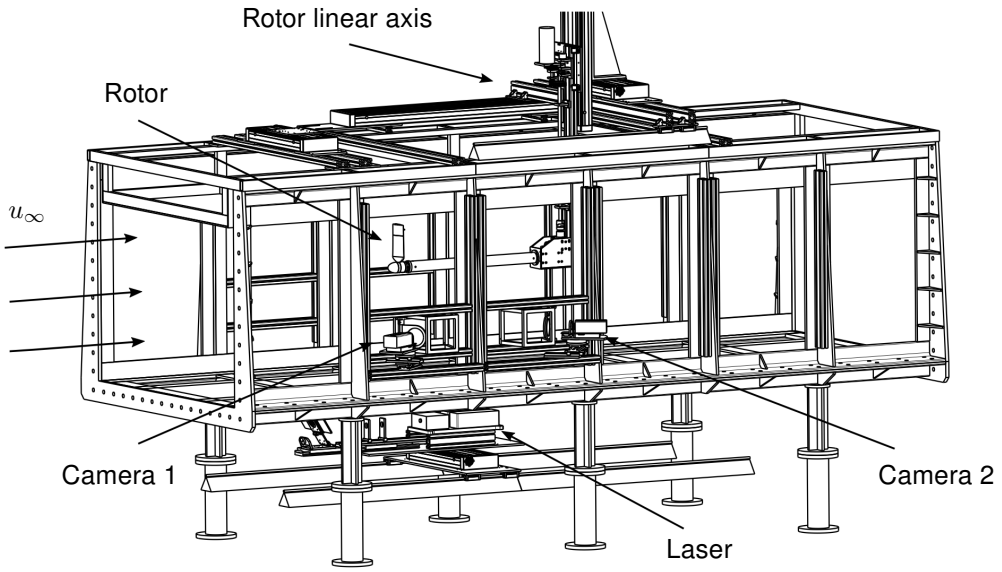

FIG 3. Schematic of the rotor configuration and Stereo-PIV setup in the water channel.

velocity. Meunier et al. [18] trace this observation to the large decrease of the maximum vorticity, which is almost conserved in the two-dimensional case. The above findings mainly involve co-rotating vortices of equal strength. Configurations consisting of unequal vortex pairs can produce different merging phenomena, such as partial straining-out or partial merging; detailed descriptions can be found in the work of Dritschel & Waugh [34] and Brandt & Nomura [35]. The asymmetry leads to a stretching and ultimate collapse of the weaker vortex in the strain field generated by the stronger vortex. In comparison to a complete merging process, the effects on the core radius and the tangential velocities of the remaining vortex are much smaller.

To gain further insight into the dynamics and the instability mechanisms occurring in helical vortex systems, the TWIN-HELIX project combines experimental and theoretical methods. It focusses on a novel generic configuration consisting of two closely spaced helical vortices, and aims at a physical understanding of the interaction mechanisms of these vortices. Several configurations with different initial vortex pair parameters are examined, with respect to various interaction mechanisms, such as long- and shortwave instabilities and merging. The primary objective is the formation of a final vortex with a larger core radius and reduced velocity gradients after the interaction of the initial vortices. Therefore, a configuration with two like-signed helical vortices of approximately equal strength is the desired outcome.

2. EXPERIMENTS

A rotor consisting of a single, slightly twisted, rectangular blade with a NACA0012 profile, a radius $r = 24$ cm and a tip chord $c_{\mathrm{tip}} = 8$ cm is investigated in a recirculating water channel in the hover regime. The simple rectangular blade geometry was chosen in order to focus on the basic mechanisms of generating two tip vortices. The large chord is used to ensure a sufficiently large core size of the tip vortex for resolved PIV in the core region. The dimensions of the test section are 1 m $\times$ 1.5 m $\times$ 6 m. A schematic representation of the experimental setup is shown in Fig. 3. The positions of both the rotor and the laser for PIV velocity measurements (see below) are controllable by a variety of linear axes. The rotor frequency was $f = 1$ Hz, resulting in a Reynolds number based on the chord and the tip speed of Re =120,000. To ensure a stationary flow around the rotor, a small free-stream velocity u_∞ in the water channel is needed to prevent the flow from recirculating around the rotor disk.

A parametric fin is placed near the tip of the blade, in order to generate a concentrated secondary vortex close to the blade tip vortex. Similar to the blade, the fin is rectangular, with a NACA0012 cross-section profile and a rounded tip. The various parameters defining the fin geometry and position are specified in Fig. 4, the fin being mounted on the pressure side of the blade. Various parameter combinations can be tested. For each case, a separate blade tip is manufactured by 3D-printing.

The rotor and fin designs were based on the results of two preliminary studies. The principle of generating tip vortex pairs with a perpendicular fin was first explored experimentally using a rectangular fixed-wing geometry. An extended parameter study lead to the identification of promising configurations producing vortex pairs of similar circulations [36]. Based on these results, the geometry of the rotating blade was designed, aiming to reproduce the distribution of bound circulation along the fixed wing in the tip region. This design, including fins, was then tested and shown to work in experiments at smaller scale (1:3).

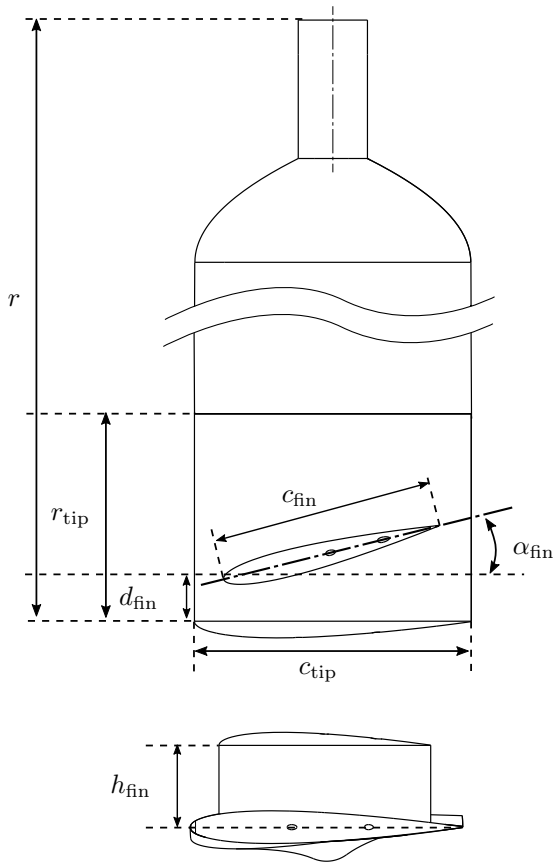

FIG 4. Blade geometry. The blade tip is interchangeable and manufactured by 3D-printing.

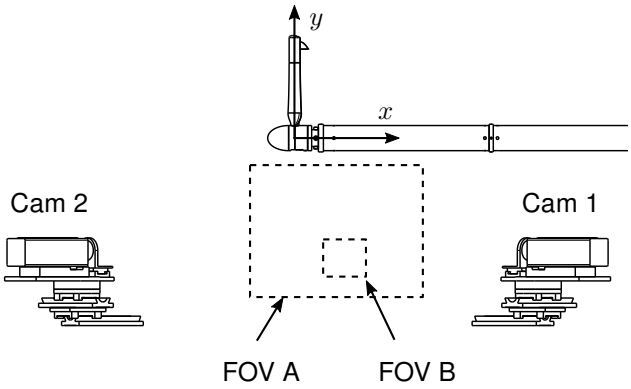

FIG 5. Coordinate system and field of views (FOV) for the PIV measurements.

Dye visualizations were carried out to examine the spatial evolution and interactions of the initial vortex system. In addition to qualitative information, knowledge about the vortex positions at different rotor phases was the second objective. Two internal channels in both blade and tip were used to inject the dye into the flow. The rotor was designed with a hollow shaft to allow the dye feed through internal tubes. A controllable linear axis was used to adjust the volumetric flow rate to the rotational speed of the rotor. Images were recorded at a frame rate of 70 Hz using a 12 megapixel XIMEA CB120xG-CM camera. Stereoscopic PIV images were recorded by two CCD cameras (PCO.2000) with a resolution of 2048×2048 pixels. Following the recommendation of Lawson & Wu [37], both cameras had a collective angle of approximately 30°. To prevent aberrations due to the change of fluids in the optical path, water-filled prisms were used, as suggested by Prasad & Jensen [38] for optical measurement techniques in water channels. The flow was illuminated by a double-pulsed laser (Quantel Twins Ultra) providing a pulse energy of 120 mJ operating at an effective wave-length of 532 nm. Cubic polyamide particles of mean diameter 50 μm and density 1.016 g/cm^3 were used to seed the flow. To prevent peak-locking errors, the foci were adjusted to secure a mean particle diameter of 2 mm in the recorded images [39]. The recordings for each plane were synchronised with the rotor frequency via an optical encoder, combined with a micro-controller to ensure exact triggering of the cameras and laser. Both the entire rotor wake and a close-up field of view containing the vortex interaction with high spatial resolution were investigated with Stereo-PIV. In a first step, a wide field of view (FOV A), mapping a 300 mm × 220 mm region of the flow was used to evaluate the spatial evolution of the vortex core positions. For a higher resolution, a second field of view (FOV B) with an edge length of 80 mm was captured. In Fig. 5, the position of both fields of view relative to the rotor are displayed.

For calibration, image acquisition, synchronisation of light source and cameras, as well as for image processing, the DaVis 8.4 software developed by LaVision was used. The light sheet was positioned directly below the axis of the rotor shaft. Using the spatial information from FOV A, the rotor was adjusted in its x- and y-position so that the vortices were always well-centred in the frame. Phase-averaged measurements unisng 250 frames were performed in $18°$-steps of the rotor angle (wake age) to give an insight into the temporal and spatial evolution of the interaction process.

3. RESULTS AND DISCUSSION

The results presented in this paper focus on a particular configuration with the following geometric parameters: c_{fin} = 64 mm, d_{fin} = 16 mm, h_{fin} = 24 mm, α_{fin} = 14°. These values produce a pair of initial vortices with a circulation ratio of approximately 1, which is the most effective value for producing a large core size after merging. Other parameter sets and a sensitivity analysis regarding the initial vortex system will be presented in future publications. A qualitative analysis of the vortex structure can be obtained from dye visualizations. Information about the initial position and spatial evolution of the vortex system provides valuable information for the subsequent PIV measurements.

Figure 6 shows the helical vortex generated by the unmodified blade. The free-stream velocity was u_∞ = 5.7 cm/s, resulting in a tip speed ratio of $\lambda = 26$. The formation of a concentrated, stable tip vortex is visible, its core dimensions seem to grow

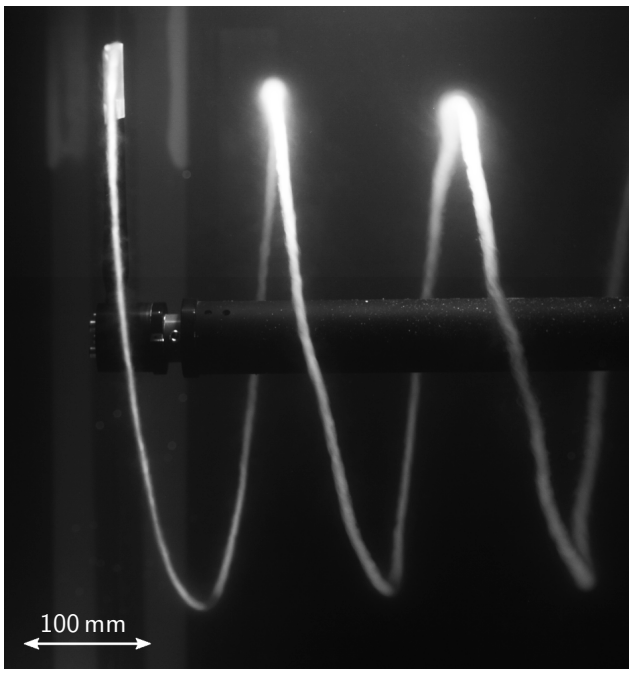

FIG 6. Dye visualization of the rotor wake for the unmodified blade, flow is from left to right.

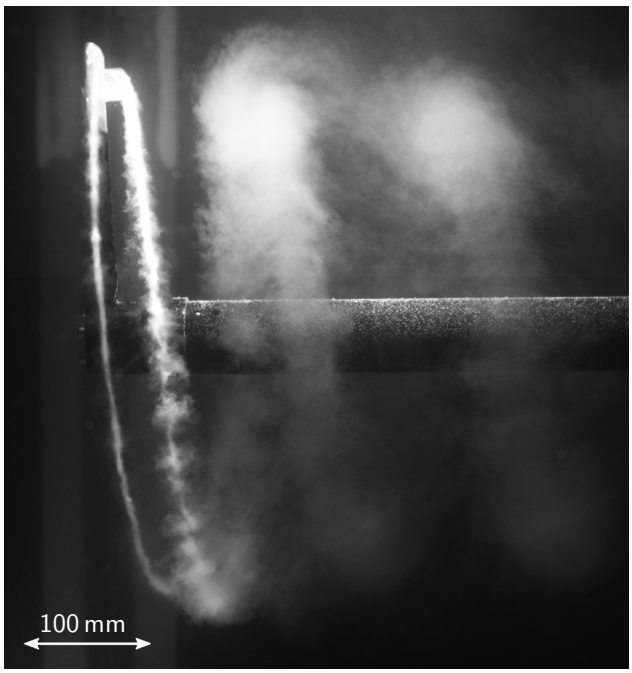

FIG 7. Dye visualization of the rotor wake for the modified blade, flow is from left to right.

.

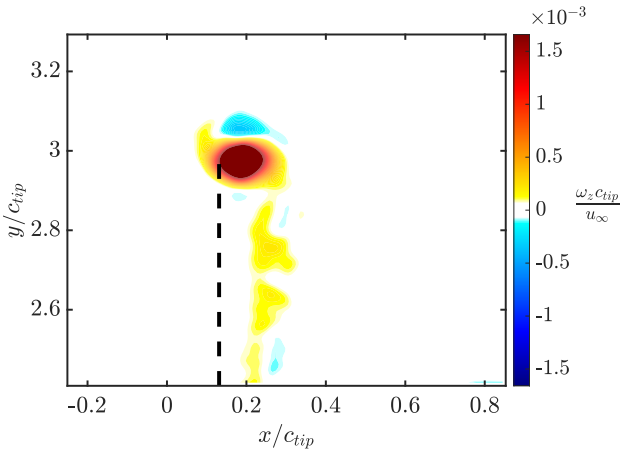

FIG 8. Phase-averaged vorticity in the centre plane of the rotor for the unmodified blade at $\phi = 18°$. The dashed line represents position of the trailing edge of the blade for $\phi = 0°$.

slightly after two revolutions. Considering the core evolution, a disturbance affecting the overall helix geometry is visible in the later stages. The extremely low free-stream velocity used in this case causes non-uniformities over the rotor diameter. Parts of the vortex are transported with slightly higher velocities, causing the visible deformation of the helix. The disturbance is not related to any long-wavelength instability phenomenon.

In comparison to the unmodified blade, the rotor wake of the modified blade shows clear differences. A result of the visualization with the same flow parameters is displayed in Fig. 7. In addition to the primary vortex generated at the blade tip, a like-signed secondary vortex is emerging from the fin tip. This secondary vortex appears to be less stable than the primary one, indicated by the disturbed dye filaments in the core region. After one revolution, the two initial vortices have merged into a single one. Visually, the core of the final vortex appears to be strongly widened, compared to the unmodified case in Fig. 6. Due to the rapid diffusion of the dye, a quantitative analysis of the core dimensions is not feasible. Nevertheless, the results demonstrate the functionality of the performed tip modification concerning the formation of two distinct vortices, and indicate that the desired vortex interaction takes place.

The PIV analysis provides detailed quantitative information supporting the visual impressions. The results were used to determine the base flow properties of the rotor wake. In the close-up field of view B, the vortex evolution is recorded over one rotor revolution in steps of 18°. In Fig. 8, the phase-averaged vorticity in a plane containing the rotor axis, obtained from 250 instantaneous fields, is plotted for the unmodified rotor at $\phi = 18°$. The single, concentrated vortex emerging from the blade tip is clearly visible, the roll-up process is completed. The unmodified case acts as the reference in this study. Regarding the growth of the vortex cores, the findings of the PIV results show good agreement with the theoretical predictions. The radius of the tip vortex core ($a_{\max}$) is the distance from the vortex centre where the swirl velocity is maximal. The equivalent Gaussian vortex core radius is then defined as $a = a_{\max}/1.12$ (see, e.g., [14]). In Fig. 9, the evolution of the normalized Gaussian core radius with the rotor phase is plotted. The dashed line represents the laminar growth due to viscous diffusion of a two-dimensional Gaussian vortex core:

$$a = \sqrt{a_0^2 + 4\nu t}. \tag{1}$$

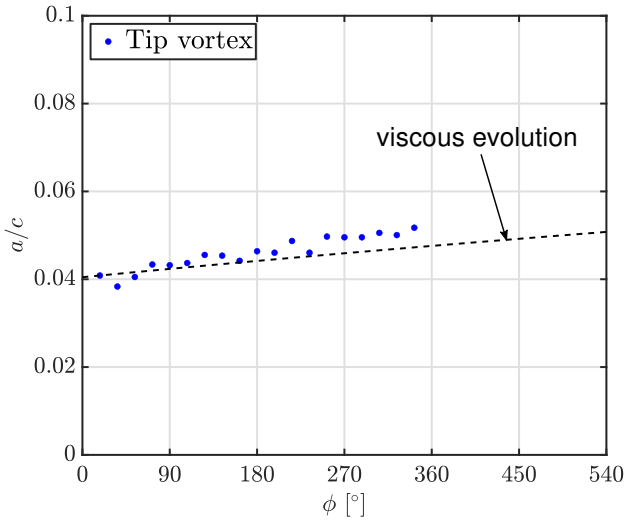

FIG 9. Core radius evolution for the tip vortex of the unmodified blade.

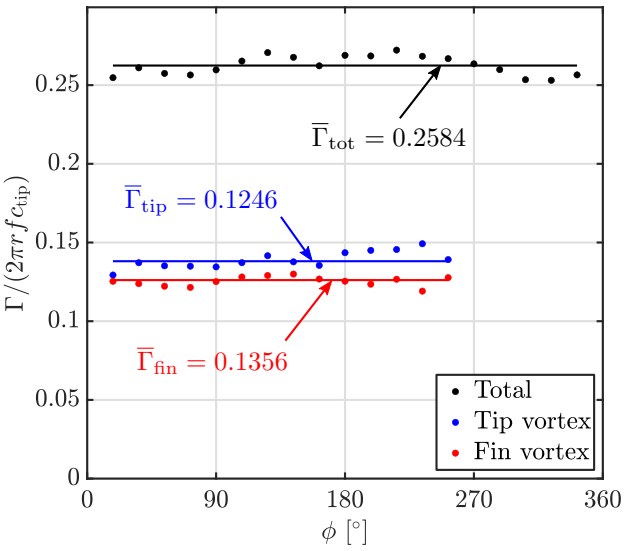

FIG 11. Vortex circulations for the modified blade.

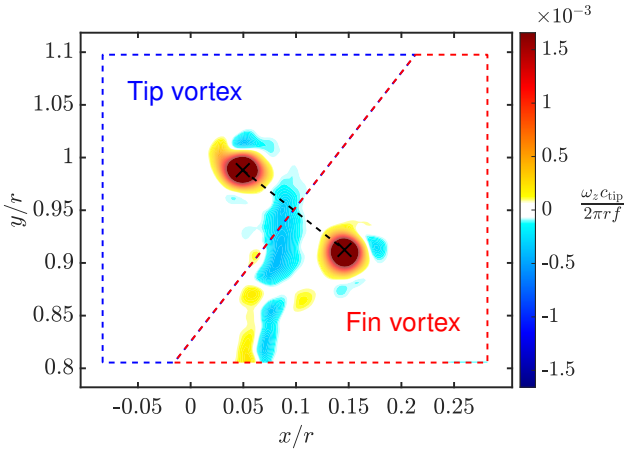

FIG 10. Phase-averaged vorticity for the modified blade ($\phi = 18°$). Blue and red polygons show the integration regions for the circulation calculation.

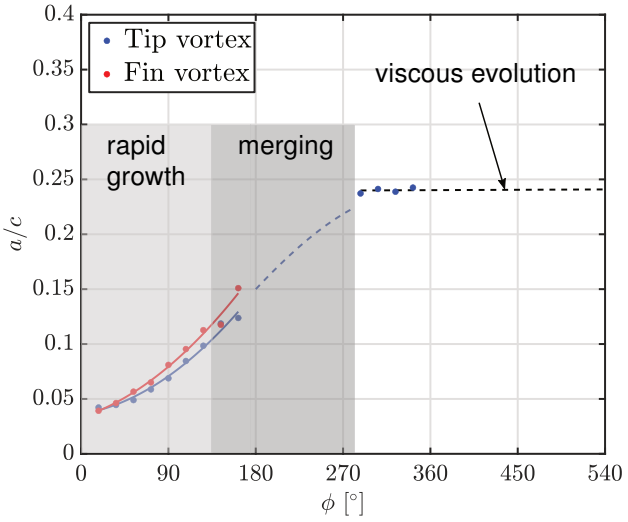

FIG 12. Core radii evolution leading to the eventual vortex merging for the modified blade.

Comparison between the predicted growth rate and the experimental data shows good agreement. This indicates that, despite the fairly high Reynolds number, the inner core region is laminar. The tip vortex also possesses a velocity component along its axis. This feature and its influence on possible instability mechanisms will be analysed in forthcoming studies.

The initial vortex system emerging from the modified blade differs significantly from the reference case. Two distinct vortices of similar size are generated at the tip and the fin, which form a co-rotating vortex system prone to vortex merging. Figure 10 shows the corresponding vorticity field. This figure also illustrates how the circulation of each individual vortex was determined: the vorticity field is separated into two distinct regions, marked by the blue and red polygons. Each vortex centre is determined using the λ_2-criterion defined by Jeong & Hussain [40]. A separation line is drawn orthogonally to the line connecting the centres, allocating the vorticity in the respective region to the tip or the fin vortex.

Figure 11 shows the circulations found in this way for an entire revolution. The individual quantities and the total circulation based on the entire field of view are plotted over the rotor phase ϕ. It is notable that both vortices produce almost the same circulation, making this configuration suitable for a complete merging process. The ratio of the average circulations of the two vortices is $\overline{\Gamma}_{\mathrm{fin}}/\overline{\Gamma}_{\mathrm{tip}} \approx 0.9$. At a rotor phase of $\phi = 270°$, the merging process is almost completed and two distinct vortex centres cannot be detected anymore.

The development of the core radii in the modified case is displayed in Fig. 12, which shows strong differences to Fig. 9. Both vortices exhibit an immediate rapid growth of their core radii, visible from $\phi = 18°$ up to $\phi = 180°$. The conglomeration of the vortices, starting at approximately $\phi = 180°$ inhibits a valid detection of the core radii since a precise peak in the tangential velocity cannot be detected anymore.

In Fig. 13, the evolution of the ratio between Gaussian core radii and the core separation distances is plotted over the rotor phase. Meunier et al. [30] found that for

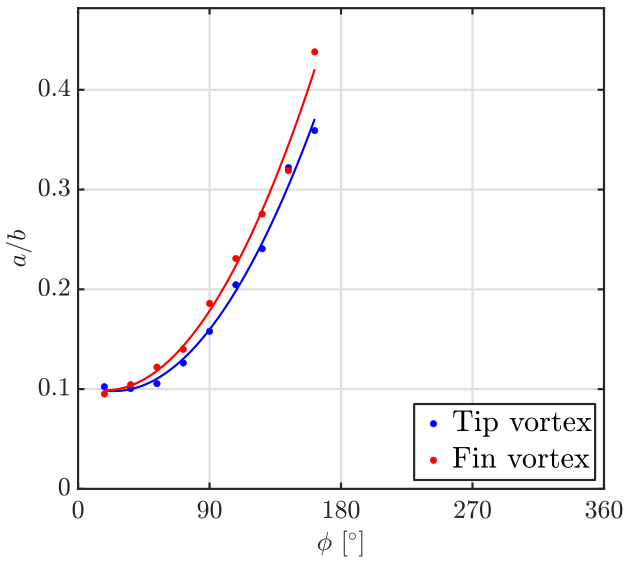

FIG 13. Evolution of the ratio between Gaussian core radii and core distance.

two-dimensional co-rotating vortices, merging sets in when this ratio exceeds $a/b \approx 0.24$. Below this value, one observes a slow increase, due to the growth of the core radius on a viscous time scale (see Eq. (1)), whereas the separation distance b remains essentially constant. The rapid increase observed in Fig. 13 well before reaching $a/b = 0.24$ indicates the presence of a perturbation or instability having a significant influence on the growth of the core radii. Fig. 14 shows the vortex system before the critical ratio is reached at a rotor phase of $\phi = 126°$. Both vortices have similar circulation (Fig. 11), and rotate around each other while moving downstream. The rapid growth of the core size is qualitatively visible. Meunier et al. [30] pointed out the significant influence of the elliptic instability on the merging process [30]. Considering the high Reynolds number at the blade tip ($Re = 120,000$), mutual instabilities affecting the growth rates of the radii might occur in the initial stages of the flow. A detailed analysis of the instability phenomenon arising in this configuration will be performed in further studies. The presence of the instability accelerates the core growth and therefore the onset of the merging process. Fig. 15 shows vorticity fields during merging. A deformation of the vortex structure combined with a decrease of the core separation occurs, resulting in the combination of both vortices into a single one. During this process, the vortex centres and core radii cannot be accurately detected in the experimental measurements, which explains the missing information in the merging region in Fig. 12. After completion of the merging process (at $\phi \approx 290°$), the final vortex has a normalised core radius $a/c \approx 0.245$. From this point onwards, the growth follows again the viscous diffusion law in Eq. (1). In relation to the initial state, the core size is multiplied by a factor of about 5. Meunier et al. [30] found a factor of 3.5 for the merging of straight co-rotating vortices under the influence of elliptic instability, and a factor of 1.5 for the unperturbed case. The large growth found

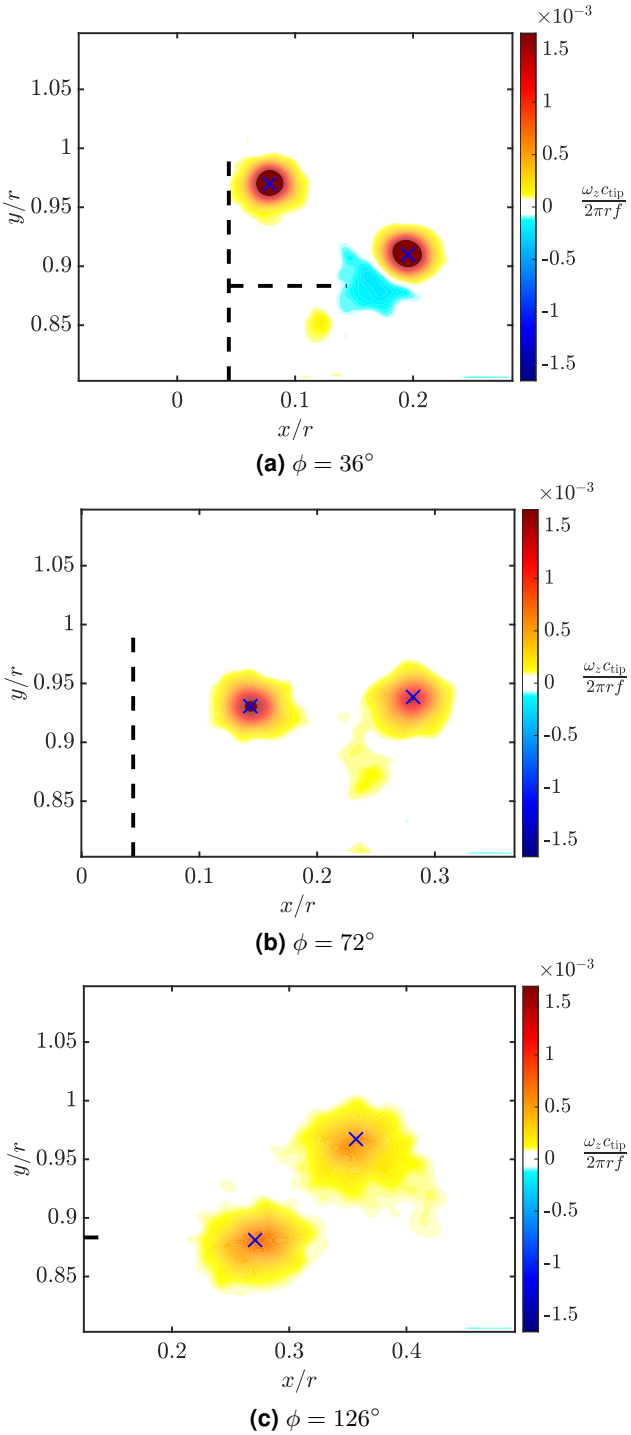

(a) $\phi = 36°$

(b) $\phi = 72°$

(c) $\phi = 126°$

FIG 14. Phase-averaged vorticity before the onset of merging for the modified blade. The dashed lines represent the trailing edges of the blade and the fin.

in the present configuration therefore underlines the probable presence of an instability.

The strong increase in core size is accompanied by a decrease of the peak vorticity, due to the conservation of circulation. In addition, the tangential (swirl) velocities in the vortices are strongly influenced by the merging process. The evolution of the maximum tangential velocity for both tip and fin vortex is plotted in Fig. 16. An abrupt decrease is notable in both vortices, corresponding to the rapid core growth in

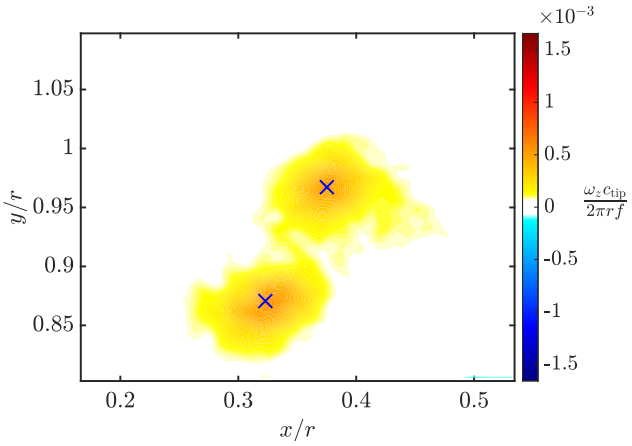

(a) $\phi = 144°$

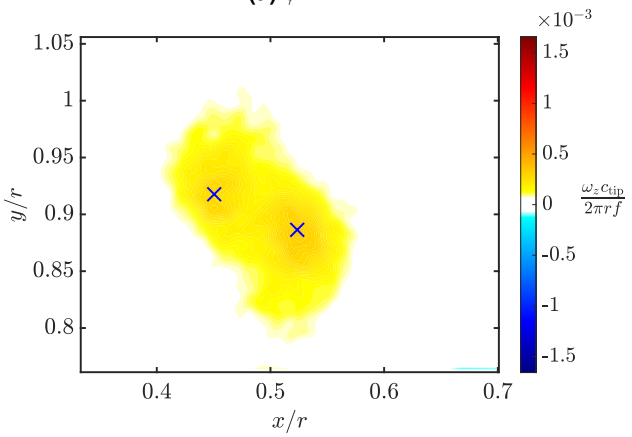

(b) $\phi = 216°$

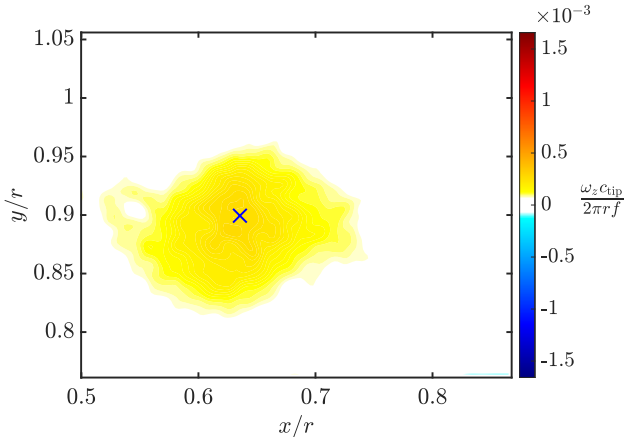

(c) $\phi = 288°$

FIG 15. Series of contour plots illustrating the merging process.

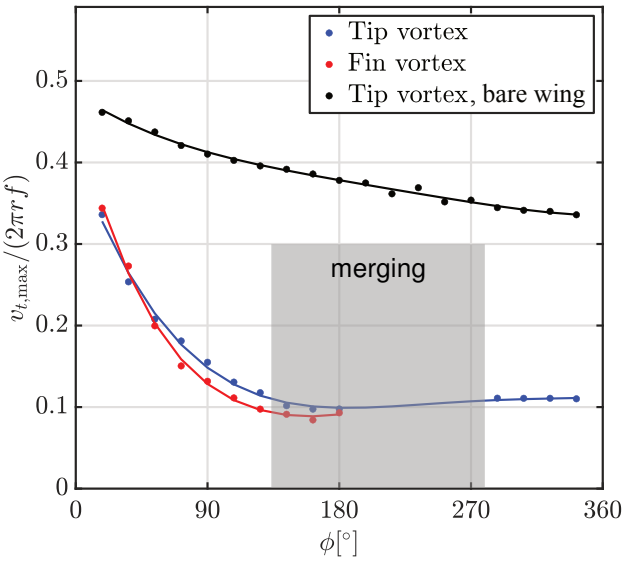

FIG 16. Maximum values of the tangential velocity v_t for tip and blade vortex, plotted for one rotor revolution.

Fig. 12. The maxima decrease down to 30% of the initial values at a rotor phase of $\phi \approx 160°$. Once the vortices have merged, the peak velocity of the final vortex remains essentially constant. The single vortex from the unmodified blade shows only a slight decrease during the first rotor period. After one revolution, the peak velocity of the merged vortex is about 3.5 times lower than for the reference case.

A visual illustration of the differences between both final vortices is given by the vorticity fields in Fig. 17. Whereas the presence of the tip fin strongly modifies the core size, vorticity and swirl velocities of the rotor wake vortices, the large-scale spatial structure of the vortex system is nearly unaffected. The positions of the vortex centres after one blade rotation are almost identical for both cases. Considering the initial objective of the blade tip modification, the desired effect on the vortex properties responsible for the negative effects of BVI, i.e. the increase of the core size and reduction of velocity gradients, was achieved.

4. CONCLUSION

We have presented the results of an experimental study of two closely spaced helical vortices, created by a generic rotor blade equipped with a parametric fin. The objective was to modify the properties of the rotor wake vortex system, in order to reduce the negative effects of blade-vortex interactions that may appear in certain regimes of rotor operation. Splitting the single concentrated blade-tip vortex into two separate co-rotating vortices was expected to produce a final merged vortex with a larger core size and lower gradients, which is beneficial for BVI. The present study has shown that this goal can be achieved with the proposed new blade tip geometry. By placing a perpendicular fin on the pressure side of the blade, a strong secondary vortex appears. Variation of the fin position and geometry allows to change the vortex parameters, and in particular to produce pairs of vortices having almost the same circulation. Dye visualizations and velocity measurement were carried out in a water channel to describe and analyse this phenomenon. They revealed that the merging process evolves surprisingly fast, indicating the presence of an instability causing an early rapid core growth. The merged vortex after one rotor rotation is found to be 5 times lager than the one shed without a fin, with a significantly reduced peak tangential velocity.

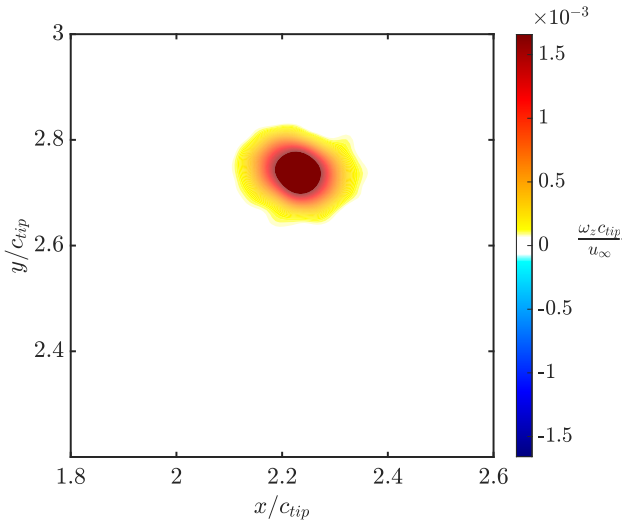

(a) Unmodified blade

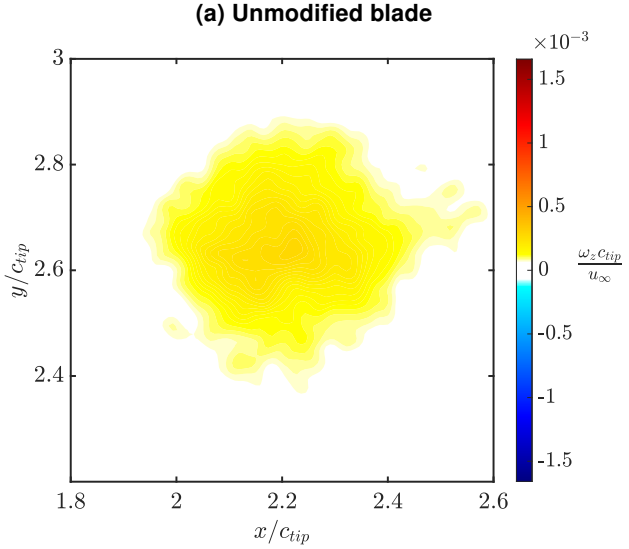

(b) Modified blade

FIG 17. Comparison of the vortex structure after one revolution. Phase-averaged vorticity at $\phi = 342°$.

Further work will include a systematic parameter study concerning the variation of the fin geometry and an investigation of the instability mechanism responsible for the rapid initial core growth observed with the modified blade. For this, volumetric PIV measurements and supporting numerical calculations also are planned.

ACKNOWLEDGMENTS

This work is part of the German-French project TWINHELIX, supported by the *Deutsche Forschungsgemeinschaft* (grant no. 391677260) and the French *Agence Nationale de la Recherche* (grant no. ANR-17-CE06-0018).

Contact address:

schroeder@ilr.rwth-achen.de

References

[1] Y. Yung, “Rotor blade–vortex interaction noise,” *Progress in Aerospace Sciences*, vol. 36, no. 2, pp. 97–115, 2000.

[2] R. Zhao, W. Shen, T. Knudsen, and T. Bak, “Fatigue distribution optimization for offshore wind farms using intelligent agent control,” *Wind Energy*, vol. 15, no. 7, pp. 927–944, 2012.

[3] F. H. Schmitz and Y. H. Yung, “Helicopter impulsive noise: Theoretical and experimental status,” *Journal of Sound and Vibration*, vol. 109, no. 3, pp. 361–422, 1986.

[4] Y. Yung, B. Gmelin, W. Splettstoesser, J. J. Philippe, J. Prieur, and T. F. Brooks, “Reduction of helicopter blade-vortex interaction noise by active rotor control technology,” *Progress in Aerospace Sciences*, vol. 33, no. 9-10, pp. 647–687, 1997.

[5] A. Brocklehurst and G. N. Barakos, “A review of helicopter rotor blade tip shapes,” *Progress in Aerospace Sciences*, vol. 56, pp. 35–74, 2013.

[6] T. Leweke, S. Le Dizès, and C. H. Williamson, “Dynamics and instabilities of vortex pairs,” *Annual Review of Fluid Mechanics*, vol. 48, pp. 507–541, 2016.

[7] T. Leweke, H. U. Quaranta, H. Bolnot, F. J. Blanco-Rodríguez, and S. Le Dizès, “Long- and short-wave instabilities in helical vortices,” *Journal of Physics: Conference Series*, vol. 524, 012154, 2014.

[8] S. E. Widnall, “The stability of a helical vortex filament,” *Journal of Fluid Mechanics*, vol. 54, no. 4, p. 641, 1972.

[9] B. P. Gupta and R. G. Loewy, “Theoretical analysis of the aerodynamic stability of multiple, interdigitated helical vortices,” *AIAA Journal*, vol. 12, no. 10, pp. 1381–1387, 1974.

[10] S. Kawada, “Induced velocity by helical vortices,” *Journal of the Aeronoutical Sciences*, vol. 1936, no. 3, pp. 86–87, 1936.

[11] J. C. Hardin, “The velocity field induced by a helical vortex filament,” *The Physics of Fluids*, vol. 25, no. 11, p. 1949, 1982.

[12] V. L. Okulov, “On the stability of multiple helical vortices,” *Journal of Fluid Mechanics*, vol. 521, pp. 319–342, 2004.

[13] H. U. Quaranta, H. Bolnot, and T. Leweke, “Long-wave instability of a helical vortex,” *Journal of Fluid Mechanics*, vol. 780, pp. 687–716, 2015.

[14] H. U. Quaranta, M. Brynjell-Rahkola, T. Leweke, and D. S. Henningson, “Local and global pairing instabilities of two interlaced helical vortices,”

Journal of Fluid Mechanics, vol. 863, pp. 927–955, 2019.

[15] D. W. Moore and P. G. Saffman, "The instability of a straight vortex filament in a strain field," *Proceedings of the Royal Society A*, vol. 346, no. 1646, pp. 413–425, 1975.

[16] R. R. Kerswell, "Elliptical instability," *Annual Review of Fluid Mechanics*, vol. 34, pp. 83–113, 2002.

[17] T. Leweke and C. H. K. Williamson, "Cooperative elliptic instability of a vortex pair," *Journal of Fluid Mechanics*, vol. 360, pp. 85–119, 1998.

[18] P. Meunier and T. Leweke, "Elliptic instability of a co-rotating vortex pair," *Journal of Fluid Mechanics*, vol. 533, pp. 125–159, 2005.

[19] C. Roy, N. Schaeffer, S. Le Dizès, and M. Thompson, "Stability of a pair of co-rotating vortices with axial flow," *Physics of Fluids*, vol. 20, no. 9, p. 094101, 2008.

[20] C. Roy, T. Leweke, M. C. Thompson, and K. Hourigan, "Experiments on the elliptic instability in vortex pairs with axial core flow," *Journal of Fluid Mechanics*, vol. 677, pp. 383–416, 2011.

[21] F. J. Blanco-Rodríguez, S. Le Dizès, C. Selçuk, I. Delbende, and M. Rossi, "Internal structure of vortex rings and helical vortices," *Journal of Fluid Mechanics*, vol. 785, pp. 219–247, 2015.

[22] F. J. Blanco-Rodríguez and S. Le Dizès, "Elliptic instability of a curved Batchelor vortex," *Journal of Fluid Mechanics*, vol. 804, pp. 224–247, 2016.

[23] Y. Fukumoto and V. L. Okulov, "The velocity field induced by a helical vortex tube," *Physics of Fluids*, vol. 17, no. 10, p. 107101, 2005.

[24] Y. Hattori and Y. Fukumoto, "Short-wave stability of a helical vortex tube: the effect of torsion on the curvature instability," *Theoretical and Computational Fluid Dynamics*, vol. 24, no. 1, pp. 363–368, 2010.

[25] Y. Hattori and Y. Fukumoto, "Modal stability analysis of a helical vortex tube with axial flow," *Journal of Fluid Mechanics*, vol. 738, pp. 222–249, 2014.

[26] F. J. Blanco-Rodríguez and S. Le Dizès, "Curvature instability of a curved Batchelor vortex," *Journal of Fluid Mechanics*, vol. 814, pp. 397–415, 2017.

[27] Y. Hattori, F. J. Blanco-Rodríguez, and S. Le Dizès, "Numerical stability analysis of a vortex ring with swirl," *Journal of Fluid Mechanics*, vol. 878, pp. 5–36, 2019.

[28] E. J. Hopfinger and G. J. F. van Heijst, "Vortices in rotating fluids," *Annual Review of Fluid Mechanics*, vol. 25, pp. 241–289, 1993.

[29] C. Cerretelli and C. H. K. Williamson, "The physical mechanism for vortex merging," *Journal of Fluid Mechanics*, vol. 475, pp. 41–77, 2003.

[30] P. Meunier, S. Le Dizès, and T. Leweke, "Physics of vortex merging," *Comptes Rendus Physique*, vol. 6, no. 4-5, pp. 431–450, 2005.

[31] M. V. Melander, N. J. Zabusky, and J. C. McWilliams, "Symmetric vortex merger in two dimensions: causes and conditions," *Journal of Fluid Mechanics*, vol. 195, pp. 303–340, 1988.

[32] P. Meunier and T. Leweke, "Three-dimensional instability during vortex merging," *Physics of Fluids*, vol. 13, no. 10, pp. 2747–2750, 2001.

[33] P. Meunier, U. Ehrenstein, T. Leweke, and M. Rossi, "A merging criterion for two-dimensional co-rotating vortices," *Physics of Fluids*, vol. 14, no. 8, pp. 2757–2766, 2002.

[34] D. G. Dritschel and D. W. Waugh, "Quantification of the inelastic interaction of unequal vortices in two–dimensional vortex dynamics," *Physics of Fluids A*, vol. 4, no. 8, pp. 1737–1744, 1992.

[35] L. K. Brandt and K. K. Nomura, "Characterization of the interactions of two unequal co-rotating vortices," *Journal of Fluid Mechanics*, vol. 646, pp. 233–253, 2010.

[36] D. Schröder, T. Leweke, R. Hörnschemeyer, E. Stumpf, "Generation of a wingtip vortex pair using a pressure-side fin," *Aerospace Science and Technology*, submitted, 2020.

[37] N. J. Lawson and J. Wu, "Three-dimensional particle image velocimetry: experimental error analysis of a digital angular stereoscopic system," *Measurement Science and Technology*, vol. 8, no. 12, pp. 1455–1464, 1997.

[38] A. K. Prasad and K. Jensen, "Scheimpflug stereocamera for particle image velocimetry in liquid flows," *Applied Optics*, vol. 34, no. 30, pp. 7092–7099, 1995.

[39] M. Raffel, C. E. Willert, F. Scarano, C. J. Kähler, S. T. Wereley, and J. Kompenhans, *Particle Image Velocimetry: A Practical Guide*. Cham: Springer International Publishing, 3rd ed., 2018.

[40] J. Jeong and F. Hussain, "On the identification of a vortex," *Journal of Fluid Mechanics*, vol. 285, pp. 69–94, 1995.